BIOLOGICAL CRYSTALLOGRAPHY

ISSN 1399-0047

Structures of the methyltransferase component of *Desulfitobacterium hafniense* DCB-2 *O*-demethylase shed light on methyltetrahydrofolate formation

Hanno Sjuts,*‡ Mark S. Dunstan, Karl Fisher and David Leys

Manchester Institute of Biotechnology, Faculty of Life Sciences, University of Manchester, 131 Princess Street, Manchester M1 7DN, England. *Correspondence e-mail: sjuts@em.uni-frankfurt.de

Received 5 May 2015
Accepted 7 July 2015

Edited by Z. S. Derewenda, University of Virginia, USA

‡ Present address: Goethe University Frankfurt, Institute of Biochemistry, Max-von-Laue-Strasse 9, 60438 Frankfurt, Germany.

Keywords: methyltransferase; *O*-demethylation; crystal structure; methyltetrahydrofolate.

PDB references: methyltransferase component involved in *O*-demethylation, 4o0q; complex with MTHF, 4o1e; complex with THF, 4o1f

Supporting information: this article has supporting information at journals.iucr.org/d

O-Demethylation by acetogenic or organohalide-respiring bacteria leads to the formation of methyltetrahydrofolate from aromatic methyl ethers. *O*-Demethylases, which are cobalamin-dependent, three-component enzyme systems, catalyse methyl-group transfers from aromatic methyl ethers to tetrahydrofolate *via* methylcobalamin intermediates. In this study, crystal structures of the tetrahydrofolate-binding methyltransferase module from a *Desulfitobacterium hafniense* DCB-2 *O*-demethylase were determined both in complex with tetrahydrofolate and the product methyltetrahydrofolate. While these structures are similar to previously determined methyltransferase structures, the position of key active-site residues is subtly altered. A strictly conserved Asn is displaced to establish a putative proton-transfer network between the substrate N5 and solvent. It is proposed that this supports the efficient catalysis of methyltetrahydrofolate formation, which is necessary for efficient *O*-demethylation.

1. Introduction

Organohalide-respiring bacteria can make use of halogenated organic molecules as terminal electron acceptors (Smidt & de Vos, 2004; Hug *et al.*, 2013). It has become apparent that the genomes of specific organohalide-respiring bacteria not only contain multiple reductive dehalogenases but also several gene clusters that encode *O*-demethylase enzyme systems (Schilhabel *et al.*, 2009; Studenik *et al.*, 2012; Kim *et al.*, 2012). *O*-Demethylases link C1 metabolism with catabolic acetyl-CoA pathways in, for example, lignin breakdown, and have previously been identified in acetogenic bacteria (Bache & Pfennig, 1981; Kaufmann *et al.*, 1997). These enzymes belong to the cobalamin-dependent methyl-transfer enzyme class (Matthews *et al.*, 2008) and catalyse methyl-group transfer from a donor to a methyl-group acceptor *via* methylcobalamin. Methyl-donor substrates for *O*-demethylases include aromatic methyl ethers (*e.g.* vanillate or syringate), and the final methyl-group acceptor is tetrahydrofolate (THF). Methylation of THF occurs at N5 of the pterin moiety of the THF substrate and results in the formation of N^5-methyltetrahydrofolate (MTHF), which can subsequently be used to synthesize acetyl-CoA (Ragsdale, 2008). Three different proteins are directly involved in *O*-demethylation: (i) the substrate-binding protein, (ii) the central cobalamin-binding protein (Sjuts *et al.*, 2013) and (iii) the THF-binding protein, which is the methyl-group acceptor.

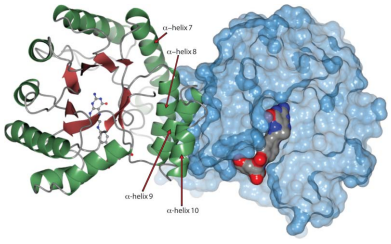

A fourth protein is thought to reactivate the cobalamin cofactor in case of oxidation to the inactive +2 redox state *via* ATP-dependent reduction to the cob(I)alamin state (Siebert *et al.*, 2005; Nguyen *et al.*, 2013). The overall reaction and the protein modules involved in *O*-demethylation are illustrated in Fig. 1(*a*). A few three-component *O*-demethylases have

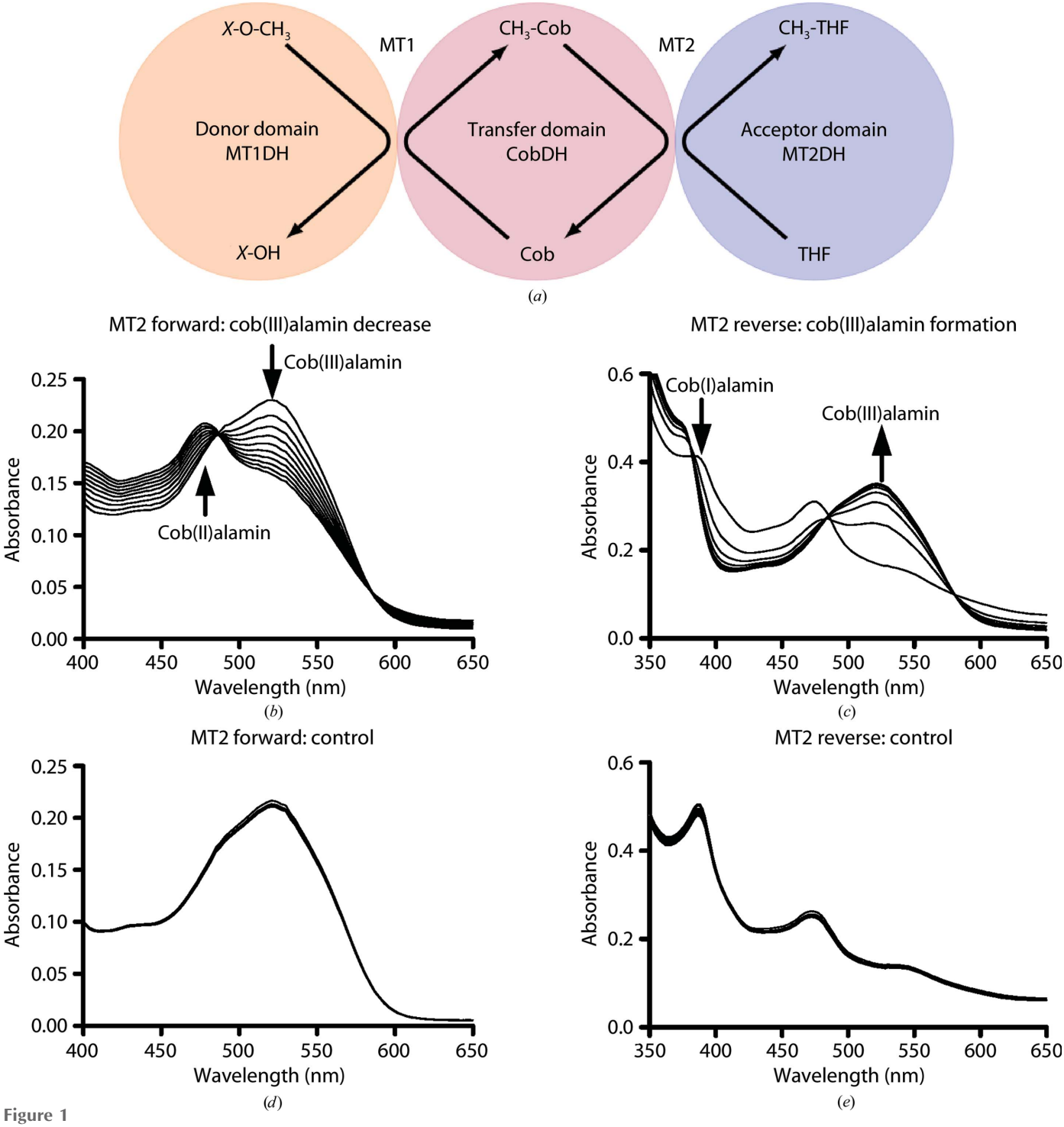

Figure 1
(*a*) Schematic illustration of the *O*-demethylation reaction and the protein components involved. The methyl-donor (substrate) binding domain is shown in orange, the cobalamin-binding domain catalysing the methyl-transfer reaction is shown in magenta and the THF-binding methyl-acceptor domain is shown in blue. MT1 and MT2 indicate the two iterative methyl-transfer reactions that occur during *O*-demethylation. (*b*) Methyltransferase reaction from methylcobalamin to THF. The methyl-transfer reaction was initiated by the addition of THF and observed by the decrease in methylcobalamin absorbance at 525 nm and the increase in cob(II)alamin absorbance at 477 nm. (*c*) MT2DH also catalyses the reverse methyl-group transfer reaction from MTHF to cob(I)alamin, resulting in methylcobalamin and THF, which is observed by a decrease in the cob(I)alamin signal at 388 nm and an increase in methylcobalamin [cob(III)alamin] absorbance at 525 nm. (*d*, *e*) No methyl transfer is observed for the forward or reverse reaction in the absence of MT2DH. Spectra were recorded every 3 min for a total of 30 min.

been isolated and characterized biochemically. The *Moorella thermoacetica* *O*-demethylase system has been shown to use dicamba and vanillate as substrates (Naidu & Ragsdale, 2001). Similar observations have been made for *O*-demethylases from *Acetobacterium dehalogenans* and *Desulfitobacterium hafniense* DCB-2 (Schilhabel *et al.*, 2009; Studenik *et al.*, 2012; Engelmann *et al.*, 2001). Aromatic methyl ethers can be highly chlorinated and it has therefore been suggested that in organohalide-respiring bacteria such as *D. hafniense* DCB-2 reductive dehalogenation and *O*-demethylation reactions occur that share the same or similar substrates (Villemur, 2013).

Interestingly, methyl transfer can in principle occur in both directions (Ragsdale, 2008). It has been observed that methyl transfer from MTHF to cob(I)alamin is reversible in methionine synthase (MetH; Goulding *et al.*, 1997). Whether individual methyltransferases have specialized to catalyse methyl transfer in a particular direction is unclear. Several methyltransfer enzymes have been studied extensively that use MTHF as the methyl-group donor, including MetH and the methyltransferase (MeTr) of the corrinoid/iron–sulfur protein (CoFeSP), which is involved in the Wood–Ljungdahl pathway of anaerobic CO_2 fixation. The crystal structures of these methyltransferases have revealed that they contain a conserved Asn residue in the proximity of the N5 atom of MTHF. This residue has been shown to be important for catalysis and has been implicated in transition-state stabilization (Evans *et al.*, 2004; Doukov *et al.*, 2007; Goetzl *et al.*, 2011). To date, no methyltransferase structures have been described for those systems that predominantly function to form MTHF from THF. In order to evaluate whether any mechanistic and structural differences occur between the two methyl-transfer directions, crystal structures of the methyl-group acceptor protein (MT2DH) from a putative *O*-demethylase from *Desulfitobacterium hafniense* DCB-2 in the apo form and in complex with THF and MTHF have been solved. Interestingly, the MT2DH crystal structures suggest that the conserved Asn residue (Asn199 in MT2DH) is not directly involved in methyl-group transfer.

2. Materials and methods

All chemicals used in this study were purchased from Sigma–Aldrich unless stated otherwise.

2.1. Cloning and overexpression of MT2DH

Genomic DNA from *D. hafniense* DCB-2 was used as a PCR template for amplification of the *Dhaf0722* gene (encoding MT2DH) with 5′ overhangs that are compatible with ligation-independent cloning (Takara Bio Inc.). *Dhaf0722* was inserted into the pET-28a(+) vector (Novagen) encoding an N-terminal His_6 tag and a thrombin protease cleavage site using the NdeI and BamHI restriction sites. *Escherichia coli* BL21 (DE3) cells (Merck) were transformed with the generated plasmid. For overexpression, cells were grown (750 ml cell culture in 2 l flasks) in LB medium (Formedium) including kanamycin (50 µg ml^{-1} as a selective reagent) at 37°C and shaken at 200 rev min^{-1} until they reached mid-log phase. At this point the temperature was lowered to 22°C and protein overexpression was induced by the addition of IPTG (0.2 m*M* final concentration). Cells were harvested by centrifugation after 16 h and stored at −20°C.

2.2. Purification of MT2DH

Cell pellets were resuspended (5 ml per gram of cell wet weight) in ice-cold buffer *A* [50 m*M* Tris pH 7.5, 300 m*M* NaCl, 5%(*v*/*v*) glycerol, 30 m*M* imidazole] supplemented with DNase, RNase, lysozyme and Complete EDTA-free protease inhibitor (one tablet per 50 ml; Roche) and stirred on ice for 30 min. Cells were lysed on ice by 20 cycles of sonication (15 s sonication followed by 45 s recovery time) using a Bandelin Sonopuls instrument and insoluble cell membranes were removed by ultracentrifugation at 98 000*g* for 45 min at 4°C. The soluble crude extract was loaded onto a 1 ml Ni–NTA column (GE Healthcare) equilibrated with buffer *A*. After sample loading, the column was washed with ten column volumes of buffer *A*. MT2DH was eluted using a linear gradient to buffer *B* (buffer *A* plus 270 m*M* imidazole). Fractions containing MT2DH were pooled and concentrated using a 10 kDa molecular-weight cutoff (MWCO) spin concentrator (Sartorius). MT2DH was then further purified by size-exclusion chromatography using a Superdex 200 10/300 gel-filtration column equilibrated with 25 m*M* Tris pH 7.5, 150 m*M* NaCl, 1 m*M* DTT.

2.3. MT2DH methyltransferase assay

The absorbance changes of the cobalamin cofactor associated with methyl-group transfer from exogenous cobalamin to protein-bound THF were monitored spectroscopically. The assay was performed within a glove box (Belle Technologies; O_2 < 5 p.p.m.) under anaerobic conditions and in the dark at 25°C using a Cary UV–Vis spectrophotometer situated inside the glove box. DTT was omitted from the purification buffer for the methyltransferase assay and MT2DH was made anaerobic by buffer exchange within the glove box using a PD10 desalting column (Bio-Rad). Measurements were performed in a 1 ml cuvette with a path length of 1 cm in 50 m*M* MES pH 6.8, 50 m*M* NaCl containing 5 µ*M* MT2DH protein and 20 µ*M* methylcobalamin and were started by the addition of 150 µ*M* THF (Schircks Laboratories, Switzerland). Spectra were recorded every 3 min for a total of 30 min. The methylation of THF was monitored using extinction coefficients ε of 9470 M^{-1} cm^{-1} for cob(II)alamin at 477 nm and 9100 M^{-1} cm^{-1} for cob(III)alamin at 525 nm according to Goulding *et al.* (1997). The reverse reaction [methyl-group transfer from MTHF to cob(I)alamin] was studied under the same experimental conditions. Here, 5 µ*M* MT2DH protein was mixed with 20 µ*M* hydroxocobalamin and 100 µM titanium(III) citrate to fully reduce the cobalamin to the +1 oxidation state. The reaction was started by the addition of 150 µ*M* MTHF and the associated spectral changes were recorded every 3 min for a total of 30 min. Methylcobalamin

Table 1
Crystallographic data and refinement statistics.

Values in parentheses are for the highest resolution shell.

	Apo MT2DH	MTHF–MT2DH	THF–MT2DH
Data collection			
X-ray source	I24, DLS	I04, DLS	I04, DLS
Wavelength (Å)	0.98	0.98	0.98
Space group	$P2_12_12$	$P2_12_12$	$P2_12_12$
Temperature (K)	100	100	100
Unit-cell parameters (Å)	a = 90.67, b = 119.07, c = 58.15	a = 90.3, b = 118.39, c = 57.73	a = 90.19, b = 118.24, c = 57.71
Resolution range (Å)	27.7–1.92 (1.97–1.92)	29.7–1.60 (1.67–1.60)	30.6–1.80 (1.85–1.80)
Observed reflections	48828 (2470)	81041 (4062)	57921 (2939)
Multiplicity	7.1 (6.2)	6.6 (6.2)	6.5 (6.3)
Completeness (%)	99.9 (99.8)	99.7 (97.3)	99.81 (99.8)
R_{merge}† (%)	9.5 (67.0)	6.5 (67.5)	7.7 (72.7)
$R_{p.i.m.}$ (%)	3.3 (25.1)	2.9 (32.4)	2.6 (18.2)
$CC_{1/2}$ (%)	99.8 (81.8)	99.8 (72.5)	99.9 (89.9)
$\langle I/\sigma(I)\rangle$	13.5 (3.0)	16.2 (2.6)	16.5 (2.5)
No. of proteins per asymmetric unit	2	2	2
Matthews coefficient V_M (Å^3 Da^{-1})	2.62	2.57	2.56
Solvent content (%)	53	52	52
Refinement			
Resolution (Å)	27.7–1.92 (1.97–1.92)	29.7–1.60 (1.67–1.60)	30.6–1.80 (1.85–1.80)
R_{work}/R_{free}‡ (%)	18.2/22.7 (23.1/27.6)	18.9/21.2 (26.9/30.5)	20.7/24.5 (28.1/32.3)
Modelled residues, chain *A*	Pro(−4)–Lys268	Gly2–Lys268	Met1–Lys268
Modelled residues, chain *B*	His0–Leu267	His0–Leu267	Met1–Leu267
No. of protein atoms	4034	4145	4065
No. of ligand atoms	0	66	64
No. of water atoms	412	383	270
B-factor analysis			
Wilson *B* factor (Å^2)	17.8	18.7	20.5
Average *B* factor (Å^2)			
All atoms	23.6	22.3	21.7
Protein	22.7	21.0	21.0
Ligand	—	25.6	30.3
Solvent	33.1	35.5	31.0
Ramachandran statistics (%)			
Favoured	97.78	98.89	97.56
Allowed	2.04	1.11	2.44
Outliers	0.18	0	0
R.m.s.d., bond lengths (Å)	0.025	0.026	0.019
R.m.s.d., bond angles (°)	1.91	2.5	2.12
PDB code	4o0q	4o1e	4o1f

† $R_{merge} = \sum_{hkl}\sum_i |I_i(hkl) - \langle I(hkl)\rangle|/\sum_{hkl}\sum_i I_i(hkl)$, where $\langle I(hkl)\rangle$ is the mean intensity after rejections. ‡ $R_{work} = \sum_{hkl} ||F_{obs}| - |F_{calc}||/\sum_{hkl} |F_{obs}|$. R_{free} is the cross-validation R factor for the test set (5%) of reflections omitted in model refinement.

formation was monitored using an extinction coefficient ε of 9100 M^{-1} cm^{-1} for cob(III)alamin at 525 nm according to Goulding *et al.* (1997). No methyl transfer was observed in either direction in the absence of MT2DH.

2.4. Crystallization

2.4.1. Apo MT2DH. Full-length MT2DH protein including the N-terminal His_6 tag and thrombin cleavage site was concentrated to 7–8 mg ml^{-1} in gel-filtration buffer (10 m*M* Tris pH 7, 100 m*M* NaCl, 1 m*M* DTT). Crystallization screening was performed at 4°C by the sitting-drop vapour-diffusion method and drops were dispensed using a high-throughput liquid-handling robot (Mosquito MD11-11, Molecular Dimensions) in a 96-well format (200 nl protein plus 200 nl mother liquor equilibrated against 50 µl mother liquor in the reservoir well). Crystals grew in multiple conditions from the commercial crystallization screens that were tested (PACT, JCSG, Morpheus, Clear Strategy Screen I and Clear Strategy Screen II, all from Molecular Dimensions). Plate-shaped crystals grew within 72 h in a precipitant solution consisting of 100 m*M* Tris pH 7.5, 100 m*M* succinic acid, 15%(*v*/*v*) PEG 3350. These crystals were cryoprotected by transferring them briefly into reservoir solution additionally containing 20% PEG 200 before being looped and flash-cooled and stored in liquid nitrogen until measurement.

2.4.2. MTHF–MT2DH. Lyophilized methyltetrahydrofolate (MTHF; Sigma) was directly added (to a final concentration of ∼1 m*M*) to the precipitant solution that yielded the best diffracting apo MT2DH crystals [100 m*M* Tris pH 7.5, 100 m*M* succinic acid, 15%(*v*/*v*) PEG 3350]. Crystallization trials (sitting-drop vapour-diffusion technique, 2 µl total volume equilibrated against 50 µl reservoir solution) were manually set up in a cold room at 4°C with this precipitant solution using different ratios of protein solution (7–8 mg ml^{-1}) to precipitant solution ranging from 0.5:1.5 µl to 1.5:0.5 µl. Again, plate-shaped crystals grew within 72 h in several of these drops. Crystals were cryoprotected by transferring them into the corresponding mother liquor supplemented with 20% PEG 200 and a tiny amount of freshly dissolved MTHF powder to ensure the complete reconstitution of MT2DH with MTHF. After a few minutes the crystals were looped and flash-cooled and stored in liquid nitrogen until measurement.

2.4.3. THF–MT2DH. Plate-like crystals of apo MT2DH were grown as described above. An 8 µl cryoprotection solution drop was prepared from mother liquor additionally containing 19% PEG 200 and 4 m*M* THF (Schircks Laboratories, Switzerland). Single crystals were soaked in this solution for a few minutes before being looped and flash-cooled and stored in liquid nitrogen until measurement.

2.5. Data collection

Complete data sets were collected from single crystals on beamlines I24 and I04 at the Diamond Light Source (DLS) synchrotron-radiation facility. Automated data processing was performed by *xia*2 (Winter, 2010). The crystals belonged to space group $P2_12_12$ and contained two molecules in the asymmetric unit. Detailed information and statistics for the

data collection of apo MT2DH, THF–MT2DH and MTHF–MT2DH are given in Table 1.

2.6. Structure determination

2.6.1. Apo MT2DH. The structure of apo MT2DH was solved by molecular replacement with the *BALBES* software (Long *et al.*, 2008), run through the *CCP*4 suite, using the structure of an MTHF-binding protein from *Clostridium thermoaceticum* (MeTrCh; PDB entry 1f6y; Doukov *et al.*, 2000) as a search model and was refined with *REFMAC* (Murshudov *et al.*, 2011; Winn *et al.*, 2011). After one round of manual model building in *Coot*, solvent water molecules were added using the automated solvent-building version of *ARP*/*wARP* (Langer *et al.*, 2008). Iterative rounds of manual building were performed in *Coot* (Emsley *et al.*, 2010) following TLS (translation, libration, screw-motion anisotropy) refinement in *REFMAC* (Murshudov *et al.*, 2011).

2.6.2. THF–MT2DH and MTHF–MT2DH. R_{free} data (imported from the apo data set in all cases) were generated using the *FREERFLAG* (import) program in *CCP*4. Subsequently, MTHF–MT2DH phases were obtained by rigid-body refinement using the final apo MT2DH dimer structure (excluding all solvent molecules) as a starting model in *REFMAC*. Electron density for MTHF was clearly visible in the $F_o - F_c$ density map directly after rigid-body refinement. The MTHF coordinates were obtained from PDB entry 2ogy (Doukov *et al.*, 2007). Superposed MTHF coordinates were copied into the MTHF–MT2DH PDB file and refined with *REFMAC*. The THF–MT2DH structure was solved in the same way as the MTHF–MT2DH structure. Water molecules were added using the automated solvent-building version of *ARP*/*wARP* (Langer *et al.*, 2008).

The final quality of all three MT2DH crystal structures was validated using *PROCHECK* (Laskowski *et al.*, 1993) and *MolProbity* (Chen *et al.*, 2010). Crystallographic figures were generated using *PyMOL* (http://www.pymol.org) or *QtMG* (from *CCP*4).

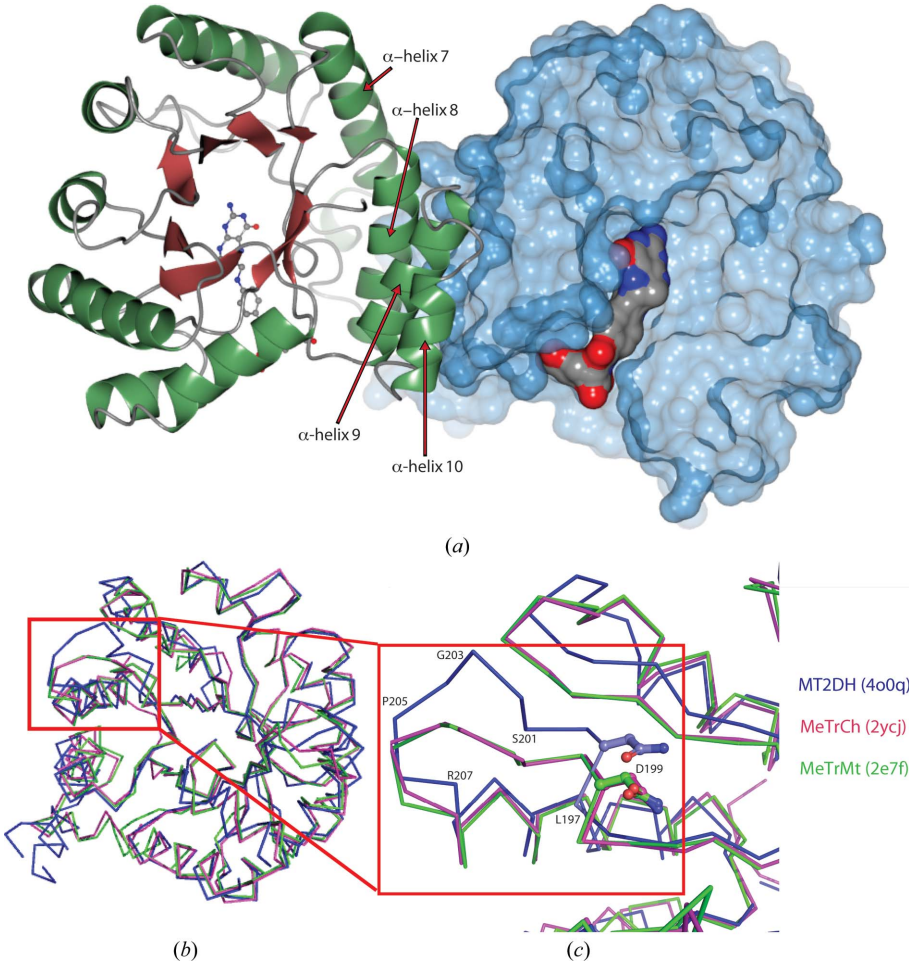

Figure 2
(*a*) The overall structure of THF–MT2DH is a homodimer. The left monomer is shown in cartoon representation with α-helices in green and β-sheets in red. α-Helices contributing to the dimer interface are indicated. The THF substrate is shown in ball-and-stick representation (C atoms, grey; N atoms, blue; O atoms, red). The right monomer is shown as a light blue surface representation with transparency set to 0.5 in order to illustrate the binding site of the THF (transparency set to 1) on a groove at the protein surface. This figure was prepared using *QtMG* from the *CCP*4 suite. (*b*) Structure alignment of methyltransferase monomers. The alignment contains the respective protein monomer chains of MT2DH (blue), MeTrCh (magenta; PDB entry 2ycj) and MeTrMt (green; PDB entry 2e7f). Protein chains are shown as C^{α} traces. (*c*) Close-up view of the protein stretch including the C-terminal end of β-strand 7 that differs in MT2DH compared with the two methyltransferase structures that catalyse the reverse reaction. The β-strand that differs between MT2DH and the other two methyltransferases in (*b*) and (*c*) is marked with red boxes.

3. Results and discussion

3.1. Methyl-group transfer from methylcobalamin to THF is catalysed by MT2DH

UV–Vis spectroscopy was used to demonstrate that the methyl group in the MT2 reaction (Fig. 1*a*) is transferred from methylcobalamin (absorbance maximum at 525 nm) to THF by MT2DH. The associated absorbance changes are shown in Fig. 1(*b*). During the methyl-transfer reaction cob(I)alamin is formed; however, owing to the lack of excess reductant in the assay mixture, cob(I)alamin is readily oxidized to cob(II)alamin (absorbance maximum of 477 nm) by trace amounts of oxygen, as observed in other studies (Studenik *et al.*, 2012). Furthermore, this demonstrates that methylcobalamin does not need to be bound to its carrier protein (in this case CobDH) for the MT2 reaction to occur. It is therefore assumed that the MT2DH protein exclusively catalyses the MT2 reaction

and that CobDH is primarily functioning as a methyl-group carrier, in agreement with other cobalamin-dependent methyltransferases (Naidu & Ragsdale, 2001; Goulding *et al.*, 1997).

Notably, MT2DH is likewise found to catalyse the reverse methyl-transfer reaction from MTHF to cob(I)alamin, as observed by the MT2DH-dependent formation of methylcobalamin from fully reduced cob(I)alamin and MTHF (Fig. 1*c*). No methyl-transfer reaction is catalysed in the absence of MT2DH (Figs. 1*d* and 1*e*). Under the conditions used, the reverse MT2 reaction (Fig. 1*c*) appears to occur faster than the forward methyl-transfer reaction (Fig. 1*b*). However, owing to the nonphysiological oxidation of the cob(I)alamin formed in the forward reaction, the rates cannot be directly compared.

3.2. Determination of the MT2DH crystal structure

MT2DH consists of 270 residues in a single polypeptide chain with a calculated molecular weight of ∼30 kDa, which is in line with SDS–PAGE analysis of the purified protein (Supplementary Fig. S1). The gel-filtration elution profile suggested that the protein forms a homodimer, similar to other methyltransferases (Goetzl *et al.*, 2011; Doukov *et al.*, 2000). Although MT2DH crystallized in several conditions, only one crystal form diffracted beyond 2 Å resolution, and this was used for all of the crystallographic experiments described here. The asymmetric unit contains two monomers related by twofold noncrystallographic symmetry, representing the dimeric form of the protein. As shown in Fig. 2(*a*), the C-terminal half of α-helix 7 and α-helices 8–10 mainly contribute to the dimer interactions. The buried surface area of the dimer interface is 2997.2 Å^2 as calculated by the *PISA* program in *CCP*4, which is similar to other methyltransferase structures, for example MeTr from *Clostridium thermoaceticum* (Doukov *et al.*, 2000).

The MT2DH monomer fold is a TIM-barrel domain consisting of eight central β-sheets surrounded by eight α-helices. The amino-acid residues of the N-terminal His_6 tag and the linker region upstream of the first residue of MT2DH (Met1) as well as at the C-terminus appear to be disordered and are therefore not visible in the electron-density map, as summarized in Table 1. The structures of THF-bound and MTHF-bound MT2DH were solved by rigid-body refinement and refined to 1.8 and 1.6 Å resolution, respectively. Electron-density maps for all three proteins are of high quality, as shown in Supplementary Fig. S2 (the N-terminus of MTHF–MT2DH chain *A*). The substrate-binding site is located on the protein surface at the C-terminal ends of the central β-sheets and is described below in greater detail. Fig. 2(*a*) shows the overall homodimer formation of THF–MT2DH.

3.3. Comparisons of the substrate-binding site of the MT2DH structure

Both monomers present in the asymmetric unit are near-identical in structure, with an r.m.s.d. value of 0.244 Å on aligning all C$^\alpha$ atoms. Structural atom alignments between MTHF–MT2DH and two other methyltransferases [MeTrCh from *Carboxydothermus hydrogenoformans* (PDB entry 2ycj; Goetzl *et al.*, 2011) and MeTrMt from *M. thermoacetica* (PDB entry 2e7f (Doukov *et al.*, 2007)] that catalyse the reverse methyl-transfer reactions have been performed. The latter are part of the Wood–Ljungdahl pathway and transfer methyl groups from MTHF to cob(I)alamin bound to a corrinoid/iron–sulfur protein (CoFeSP). The alignment (Fig. 2*b*) reveals that the structures are similar, with r.m.s.d. values of 1.059 Å (MT2DH and MeTrCh, 183 compared C$^\alpha$-atom pairs) and 1.26 Å (MT2DH and MeTrMt, 198 compared C$^\alpha$-atom pairs). All structural alignments were performed using *PyMOL*.

Fig. 3(*a*) and 3(*b*) show unbiased $F_o - F_c$ difference electron densities (green mesh, contour level 3.0σ) corresponding to MTHF and THF, respectively. Coordinated water molecules are also indicated and the side chains of Ser198 and Asn199 are shown in ball-and-stick representation.

Both MTHF and THF are very well defined in the $2F_o - F_c$ MT2DH electron density, which is shown in Fig. 3(*c*) for MTHF. The folate derivatives are bound to the protein in an elongated shape at the C-terminal ends of the central β-strands. The binding site of the pterin ring of the substrate is comprised of conserved residues and defined water molecules forming a sophisticated hydrogen-bond network. Specifically, Asp76, Asn97 and Asp161 are engaged by hydrogen bonding to the pterin heteroatoms N8, N1 and N2/N3, respectively (Figs. 3*c* and 3*d*). The water molecules W2 and W3 occupy positions similar to those observed in the MeTrMt and MeTrCh structures (Doukov *et al.*, 2007; Goetzl *et al.*, 2011).

However, some distinct differences are visible in the MT2DH structure.

The central β-strand (β-strand 7) and the adjacent C-terminal loop region (residues 190–205; MT2DH numbering) are rotated away in comparison to the corresponding regions in the two MeTr proteins (PDB entries 2ycj and 2e7f; residues 197–205; Fig. 2*c*).

It is possible that the repositioning of the residue range 197–205 in MT2DH is owing to the presence of Met204. The hydrophobic side chain of the latter appears to require a displacement of the 197–205 region to avoid steric clashes with Leu167. Alternatively, the observed difference between MT2DH and the methyltransferases could be a direct consequence of the nature of residue 177. MT2DH contains a phenylalanine at this position, whereas both of the methyltransferases contain valine residues. To accommodate the bulkier side chain of Phe177, an outward movement of helix 172–187 is required. This might in turn trigger the observed repositioning of the 197–205 region.

Intriguingly, the 197–205 region encompasses residues with potential roles in catalysis, as these are located in close proximity to the N5 atom of THF. The N5 group is methylated by methylcobalamin and the different active-site compositions between the two types of methyltransferases might reflect the fact they mainly function to catalyse methyl transfer in opposite directions.

The Asn199 residue is conserved in all reported methyltransferase crystal structures (Doukov *et al.*, 2007; Goetzl *et al.*,

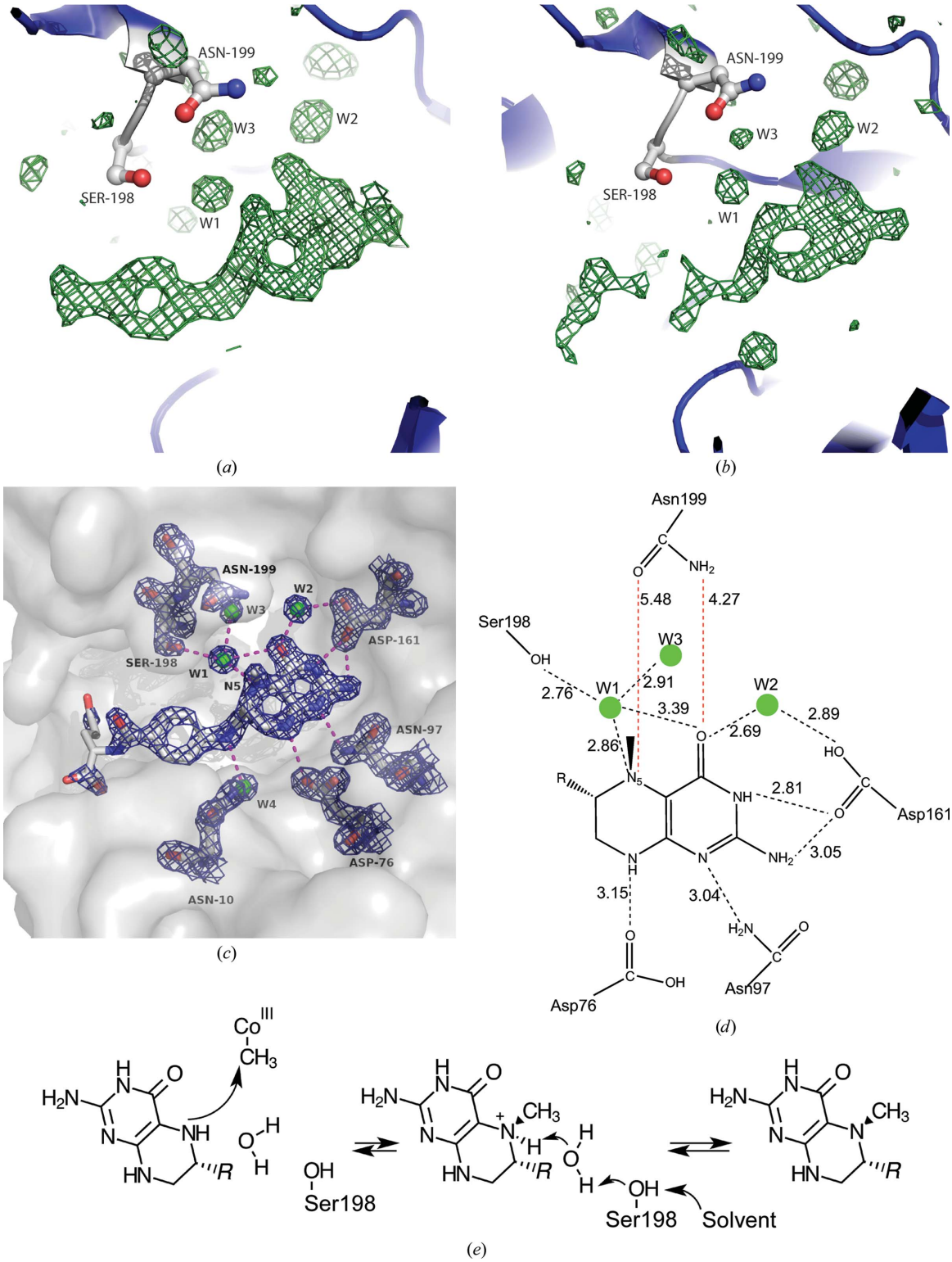

Figure 3
(*a*, *b*) OMIT $F_o - F_c$ difference electron-density maps (green mesh, contoured at 3σ) corresponding to bound MTHF (*a*) and THF (*b*). The side-chain atoms of Ser198 and Asn are shown as a ball-and-stick model (C, grey; N, blue; O, red). (*c*) The MTHF ligand bound to the typical binding site of TIM-barrel methyltransferases. MTHF and key residues implied to be important in ligand binding are shown as sticks (C, grey; N, blue; O, red). Well defined water molecules are shown as green spheres. The electron-density map ($2F_o - F_c$, contoured at 2σ) is shown as a blue mesh. All polar residues of the pterin moiety of MTHF are engaged in hydrogen bonds (indicated as magenta dotted lines). The protein surface is shown in light grey. Asn199 in this position is too distant to interact with either N5 or O4 of the MTFH substrate. (*d*) Schematic illustration of MTHF binding to MT2DH. Hydrogen bonds are shown as black dotted lines and distances are given in Å. Notably, Asn199 in both cases is too distant from the N5 atom (red dotted lines; the distance is greater than 4.3 Å) to be involved in methyl-group transfer. *R* denotes the *p*-aminobenzoylglutamate side chain of the folate. (*e*) Proposed reaction mechanism of methyl-group transfer from methylcobalamin to THF catalysed by MT2DH. *R* denotes the *p*-aminobenzoylglutamate side chain of the folate.

2011). For example, Asn199 in MeTrMt is of pivotal importance for catalysis by hydrogen bonding to the N5 atom of the MTHF substrate and is proposed to stabilize the transition state during methyl transfer (Doukov *et al.*, 2007).

In our MT2DH structures, the Asn199 residue is not within hydrogen-bonding distance of either N5 or O4 of the THF substrate (distance of ∼5 Å). Furthermore, the position of Asn199 appears to be unaffected by the binding of either THF or MTHF. This suggests that in contrast to methyltransferase enyzmes, Asn199 in MT2DH is not in a position to stabilize the transition state during methyl-group transfer between methylcobalamin and THF. Instead, a highly coordinated water molecule (W1; Fig. 3) is present in all three MT2DH structures at a hydrogen-bonding distance from N5 (3.1 Å for THF; 2.9 Å for MTHF; all quoted distances are the averages of the distances observed in each monomer). W1 in turn hydrogen-bonds to Ser198 (3.0 Å for THF; 2.8 Å for MTHF), the THF O4 atom (3.5 Å for THF; 3.4 Å for MTHF) and water molecule W3 (3.0 Å for THF; 2.9 Å for MTHF) (Figs. 3*c* and 3*d*). A water molecule has been observed in a similar position in the Asn199Ala mutant of the MeTrMt methyltransferase (W11m; Doukov *et al.*, 2007). However, in the latter the water molecule is not hydrogen-bonded to the Ser198 side chain.

3.4. Proposed reaction mechanism

While methyl-group transfers catalysed by cobalamin-dependent methyltransferases are known to be reversible (Goulding *et al.*, 1997; Seravalli, Zhao *et al.*, 1999), the reaction will predominantly occur in a particular direction depending on the metabolic pathway that it features in. During *O*-demethylation THF functions as a methyl-group acceptor, and we have shown that MT2DH catalyses both the methylation of THF by methylcobalamin as well as the reverse reaction *in vitro*. The crystal structures of MT2DH in complex with both substrate and product represent the first structures of a methyltransferase that predominantly functions to catalyse the formation of MTFH during *O*-demethylation.

Given the fact that Asn199 is not directly involved in binding to THF/MTHF, it might play only an indirect role in methyl-group transfer during *O*-demethylation. It is possible that Asn199 is important for the correct positioning of methylcobalamin prior to methyl-group transfer to N5 of THF, which is corroborated by the fact that Asn199 is highly conserved in *O*-demethylases homologous to MT2DH, as shown in Fig. 4. In MeTrMt, it has recently been proposed that Asn199, when pointing away from the active site (as in the apo MeTrMt structure), blocks the entry of cobalamin into the active site (Kung *et al.*, 2012). Upon MTHF binding and the concomitant rotation of Asn199, cobalamin binding becomes possible. Based on the MT2DH crystal structures, we propose that this mechanism does not occur in MT2DH.

The methyl-transfer potential of MTHF is intimately linked to the protonation of N5. In MT2DH, the water coordinated between Ser198 and N5 (W1) is in a position to rapidly abstract a proton from the positively charged N5 following methyl transfer, decreasing the rate of the reverse reaction from MTHF to THF. As Ser198 is located on the protein surface, it seems reasonable to assume that it is easily accessible by solvent water molecules (as illustrated in Fig. 3*e*). Furthermore, the proposed proton-relay system is in agreement with pH-dependence studies of other MTHF-dependent

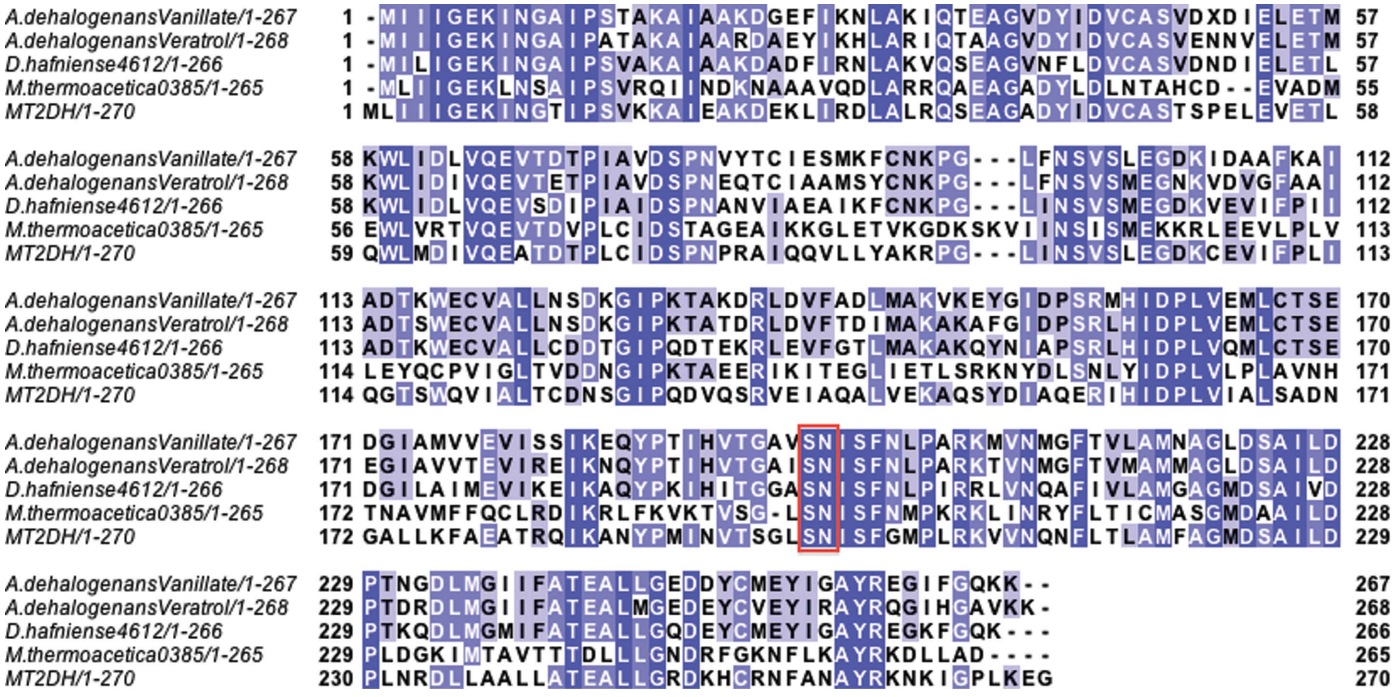

Figure 4
Protein sequence alignment between characterized methyltransferase *O*-demethylases. Ser198 and Asn199 (MT2DH numbering; highlighted by a red box) and residues 200–203 are highly conserved.

methyltransferases from *C. thermoaceticum*, which indicate that protonation of THF should decrease the rate of methyl transfer from methylcobalamin to THF (Seravalli, Zhao *et al.*, 1999; Seravalli, Shoemaker *et al.*, 1999).

4. Conclusions

This study describes the first structural characterization of a methyltransferase (MT2DH) involved in *O*-demethylation which catalyses methyl-group transfer from methylcobalamin to protein-bound THF. Although the structure of MT2DH is similar to methyltransferases that serve to catalyse the reverse reaction under physiological conditions (*i.e.* from MTHF to THF), a subtle restructuring of active-site residues (especially Ser198 and Asn199) can be observed. We speculate that displacement of Asn199 may serve to achieve the efficient catalysis of MTHF formation necessary for efficient *O*-demethylation *in vivo*. We allocate a new function to the conserved Ser198 side chain and coordinated water (W1): to act as a proton-relay network between N5 of THF and solvent during methyl-group transfer from THF to MTHF. The pK_a of N^5-methyl-THF is approximately 5.1, and only the protonated version of methyl-THF acts as a methyl donor. An efficient proton-relay system *via* W1 could serve to ensure that the rate of methyl-THF formation is increased.

Acknowledgements

The authors would like to thank Hauke Smidt for providing the *D. hafniense* DCB-2 strain. This work was supported by European Research Council (ERC) starting grant DEHALORES206080 to David Leys.

References

Bache, R. & Pfennig, N. (1981). *Arch. Microbiol.* **130**, 255–261.
Chen, V. B., Arendall, W. B., Headd, J. J., Keedy, D. A., Immormino, R. M., Kapral, G. J., Murray, L. W., Richardson, J. S. & Richardson, D. C. (2010). *Acta Cryst.* D**66**, 12–21.
Doukov, T. I., Hemmi, H., Drennan, C. L. & Ragsdale, S. W. (2007). *J. Biol. Chem.* **282**, 6609–6618.
Doukov, T. I., Seravalli, J., Stezowski, J. & Ragsdale, S. W. (2000). *Structure*, **8**, 817–830.
Emsley, P., Lohkamp, B., Scott, W. G. & Cowtan, K. (2010). *Acta Cryst.* D**66**, 486–501.
Engelmann, T., Kaufmann, F. & Diekert, G. (2001). *Arch. Microbiol.* **175**, 376–383.
Evans, J. C., Huddler, D. P., Hilgers, M. T., Romanchuk, G., Matthews, R. G. & Ludwig, M. L. (2004). *Proc. Natl Acad. Sci. USA*, **101**, 3729–3736.
Goetzl, S., Jeoung, J.-H., Hennig, S. E. & Dobbek, H. (2011). *J. Mol. Biol.* **411**, 96–109.
Goulding, C. W., Postigo, D. & Matthews, R. G. (1997). *Biochemistry*, **36**, 8082–8091.
Hug, L. A., Maphosa, F., Leys, D., Löffler, F. E., Smidt, H., Edwards, E. A. & Adrian, L. (2013). *Philos. Trans. R. Soc. Lond. B Biol. Sci.* **368**, 20120322.
Kaufmann, F., Wohlfarth, G. & Diekert, G. (1997). *Arch. Microbiol.* **168**, 136–142.
Kim, S.-H., Harzman, C., Davis, J., Hutcheson, R., Broderick, J., Marsh, T. & Tiedje, J. (2012). *BMC Microbiol.* **12**, 21.
Kung, Y., Ando, N., Doukov, T. I., Blasiak, L. C., Bender, G., Seravalli, J., Ragsdale, S. W. & Drennan, C. L. (2012). *Nature (London)*, **484**, 265–269.
Langer, G., Cohen, S. X., Lamzin, V. S. & Perrakis, A. (2008). *Nature Protoc.* **3**, 1171–1179.
Laskowski, R. A., MacArthur, M. W., Moss, D. S. & Thornton, J. M. (1993). *J. Appl. Cryst.* **26**, 283–291.
Long, F., Vagin, A. A., Young, P. & Murshudov, G. N. (2008). *Acta Cryst.* D**64**, 125–132.
Matthews, R. G., Koutmos, M. & Datta, S. (2008). *Curr. Opin. Struct. Biol.* **18**, 658–666.
Murshudov, G. N., Skubák, P., Lebedev, A. A., Pannu, N. S., Steiner, R. A., Nicholls, R. A., Winn, M. D., Long, F. & Vagin, A. A. (2011). *Acta Cryst.* D**67**, 355–367.
Naidu, D. & Ragsdale, S. W. (2001). *J. Bacteriol.* **183**, 3276–3281.
Nguyen, H., Studenik, S. & Diekert, G. (2013). *FEMS Microbiol. Lett.* **345**, 31–38.
Ragsdale, S. W. (2008). *Vitam. Horm.* **79**, 293–324.
Schilhabel, A., Studenik, S., Vödisch, M., Kreher, S., Schlott, B., Pierik, A., Pierik, A. Y. & Diekert, G. (2009). *J. Bacteriol.* **191**, 588–599.
Seravalli, J., Shoemaker, R. K., Sudbeck, M. J. & Ragsdale, S. W. (1999). *Biochemistry*, **38**, 5736–5745.
Seravalli, J., Zhao, S. & Ragsdale, S. W. (1999). *Biochemistry*, **38**, 5728–5735.
Siebert, A., Schubert, T., Engelmann, T., Studenik, S. & Diekert, G. (2005). *Arch. Microbiol.* **183**, 378–384.
Sjuts, H., Dunstan, M. S., Fisher, K. & Leys, D. (2013). *Acta Cryst.* D**69**, 1609–1616.
Smidt, H. & de Vos, W. M. (2004). *Annu. Rev. Microbiol.* **58**, 43–73.
Studenik, S., Vogel, M. & Diekert, G. (2012). *J. Bacteriol.* **194**, 3317–3326.
Villemur, R. (2013). *Philos. Trans. R. Soc. B Biol. Sci.* **368**, 20120319.
Winn, M. D. *et al.* (2011). *Acta Cryst.* D**67**, 235–242.
Winter, G. (2010). *J. Appl. Cryst.* **43**, 186–190.